DOI: 10.21062/mft.2024.059 http://www.journalmt.com

Variable Excitation Piezoelectric Energy Capture Device for Powering Scraper Conveyor Tension Detection Systems

Zhang Hezhe (0000-0002-7820-2900), Wang Cong (0000-0002-4538-0620)*
Shandong University of Science and Technology, Qingdao, China, E-mail: 1103070190@qq.com

*Corresponding author Email: 2040278481@qq.com

Past efforts which focused on the essential monitoring of the chain tension of scraper conveyers employed in fully mechanized coal mining operations have developed innovative power solutions based on the incorporation of piezoelectric devices that generate the electrical power required for the wireless transmission of chain tension data based solely on the vibrations of the scraper conveyor itself. However, these past studies have failed to evaluate the effects of different environmental factors on the electricity generating capacity of the piezoelectric devices. The present work addresses this issue by evaluating the maximum peak-to-peak voltage generated by a variable excitation piezoelectric device experimentally under a wide range of mechanical excitations, including static applied loads of 1600 g, 3200 g, and 4800 g with added oscillatory loads of different frequencies of 1.0 Hz, 2.0 Hz, and 3.0 Hz, and displacement amplitudes of 1.0 mm, 2.0 mm, and 3.0 mm. Compared with excitation frequency and excitation load the impact of an oscillatory load amplitude increasing from 1.0 mm to 3.0 mm on the obtained peak-to-peak voltages is quite profound, where the peak-to-peak voltage of the device increases by nearly 270%. The kind of piezoelectric power generation device which can adjust many kinds of external excitation is innovatively designed. The efficient and stable power supply of the piezoelectric device to the tension detection system of the scraper conveyor is realized.

Keywords: Variable excitation, Power generation characteristics, Scraper chain tension detection, Piezoelectricity ANSYS simulation

1 Introduction

Scraper conveyors play an essential role in fully mechanized coal mining operations. However, the chain tension of a scraper conveyor has a crucial impact on its working performance, where an excessive chain tension will cause the chain to break, while an overly low tension will result in poor meshing of the chain with the drive sprockets [1]. Therefore, the chain tension of scraper conveyors must be detected reliably in real time to ensure their long-term safe and stable operation [2].

This issue has been the subject of extensive investigation in recent years, and the principles and methods associated with scraper conveyor chain tension measurement are relatively well understood. For example, Mao et al. [3-5] provided a theoretical basis for conducting scraper conveyor chain tension detection by constructing a dynamic model of a scraper conveyor based on a comprehensive consideration of the nonlinearity of the chain, its elasticity, the clearance of the conveyor's middle groove, the meshing characteristics between the chain wheels and the chain, and other factors. This model was then applied for analyzing the dynamic chain tension distribution under different working conditions. Liu and Xu [6] realized the real-time detection and control of scraper conveyor chain tension by designing a scraper conveyor chain tension detection system with automatic control adjustment via an analysis and calculation of the chain tension distribution during the operation of a scraper conveyor. Liu and Yan [7] designed an automatic scraper conveyor chain tension monitoring system with a programmable logic controller (PLC) based on an analysis and calculation of the chain tension distribution during the operation of a scraper conveyor and verified the operation of the system by conducting dynamic simulations using MATLAB.

While these past studies have greatly facilitated the accurate monitoring of the chain tension in scraper conveyors, the tension data must still be transmitted by some means to operators or to chain tension control devices. This is generally conducted via wireless communication from a miniature communication device embedded in the conveyor chain. However, the rugged operating conditions and extreme space limitations of scraper conveyors greatly limit the options available for powering these communication devices. To this end, Zhang et al. [8] developed an innovative power solution based on the incorporation of a piezoelectric device that generated the electrical power required for the wireless transmission of chain tension

data based solely on the vibrations of the scraper conveyor itself. This solution enabled the reliable transmission of chain tension data over long working periods. However, this past study failed to evaluate the effects of different environmental factors on the electricity generating capacity of the piezoelectric device.

Both piezoelectric materials and piezoelectric devices have been the subject of extensive research. For example, Wilkie et al. [9] developed a new type of dense lead zirconate titanate (PZT) ceramic fiber by cutting a PZT ceramic plate with a 25–75 micron thick blade. Egusa et al. [10] successfully developed a piezoelectric composite based on an epoxy resin and PZT ceramic powders with improved electric power generation characteristics relative to those of conventional PZT piezoelectric materials. Similarly, Nhuapeng et al. [11] developed piezoelectric composites composed of an epoxy resin and 0-3 type and 1-3 type PZT powders with improved electromechanical conversion efficiency. Tanimoto [12] developed a type of carbon fiber composite reinforced with piezoelectric ceramic particles. The material was found not only to preserve the mechanical characteristics of the carbon fiber, but also provided a high level of vibration damping over a wide range of vibration frequencies, and thereby increased the voltage generated by the piezoelectric material. Cho et al. [13] deposited a monolithic single-crystal piezoelectric ceramic material onto various substrates, and analyzed the influence of electrode size, substrate thickness, piezoelectric thickness, and other parameters on the electromechanical coupling coefficient of the device. Baker et al. [14] proposed replacing a standard rectangular piezoelectric cantilever beam structure with a triangular cantilever beam structure to increase the electric power generation capabilities of piezoelectric devices. Jeon et al. [15] increased the conversion efficiency of piezoelectric wafers by designing and developing an energy collector based on a micro-electromechanical system (MEMS). The above research provides the basis for the selection of piezoelectric materials and the design of piezoelectric energy capture device.

The present work addresses the deficiency of past work by evaluating the electricity generating capacity of a variable excitation piezoelectric device experimentally under a wide range of environmental factors, including a static applied load with an additional oscillatory load of different frequencies and amplitudes. A custom-designed experimental setup is employed to enable the collection of consistent maximum and minimum voltages from the piezoelectric device under the complex static and dynamic mechanical excitations applied. The results enable the determination of the relative impacts of these various factors on the power generation performance of the piezoelectric device, and thereby facilitate the control of the electricity generating performance of the device under the actual working conditions of scraper conveyors. Accordingly, the results obtained herein enable the design of efficient piezoelectric power supplies for scraper chain tension detection systems.

2 Materials and Methods

2.1 Variable excitation piezoelectric power generating device and testing methodology

2.1.1 Working principle of device

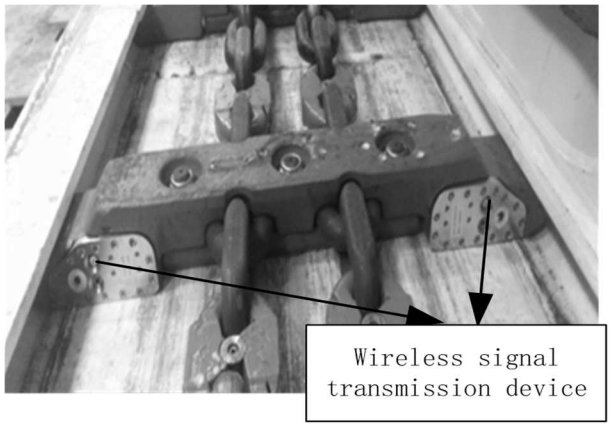

Fig. 1 *The installation diagram of the tension detection system*

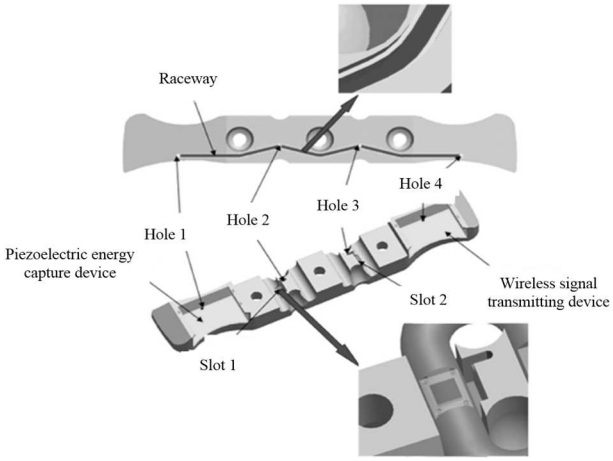

Fig. 2 *Schematic illustrating the piezoelectric power generation device*

The SGZ1000/ 1710 medium double chain scraper conveyor is adopted in the field. The installed power is 2 × 855kW, the experimental laying distance is 80m, the no-load scraper chain speed is 1.58m/s, and the no-load running time is 103s. The whole machine is laid horizontally, without installation inclination. This experiment detects the power supply of the tension sensor of the scraper conveyor. Fig. 1 shows the installation diagram of the tension detection system.

The design of the piezoelectric power generation device is illustrated in Fig. 2. As indicated, the device is placed in hole 1, and the wireless signal transmission device is placed in hole 4. The device generates electric

power via the external excitations arising from vibrations during scraper conveyor operation, and the generated power is routed to the wireless signal transmission device via wires passing through the raceway installed on the bottom of the mounting structure [16-19].

2.1.2 Variable excitation application device and piezoelectric device structure

Experimental analysis was conducted via the specially designed variable excitation application device presented in Fig. 3, Because the size of the medium voltage electrical device installed in scraper conveyor is too small, the experimental research will cause many inconvenience, which was designed with equal proportion amplification. The excitation application device is mainly composed of a frame, a bottom floor plate, a mass block, and a spring baffle. The frame is composed of four angle brackets (13 cm long and 2.0 cm wide along each side of the bracket) that are welded to the four corners of a steel plate with dimensions of 12 cm × 12 cm × 1.0 cm, which serves as the floor of the device. The piezoelectric power generation device is installed on another steel platform welded to the frame at a point groove 1cm above the top of the floor plate. This platform is composed of three steel plates with dimensions of 12 cm × 12 cm × 1.0 cm, and the ceramic piezoelectric generator device is installed underneath the bottom plate. The piezoelectric device is a single-chip ceramic piezoelectric plate with a length of 40 mm, a width of 30 mm, and a thickness of 0.3 mm. Its detailed performance parameters are listed in Table 1. As shown in Fig. 3, the two ends of the piezoelectric device are fixed onto the platform**.** The installation in Fig.4 is further clarified by the images presented in Fig. 5, where the steel blocks have cross-sectional areas of 4.0 cm × 4.0 cm and extend across the full 30 cm width of the piezoelectric chip. The steel blocks are glued to the piezoelectric chip and the supporting platform to ensure that the two ends and the middle of the piezoelectric chip are firmly fixed to the supporting platform. Wires are connected to the top and bottom surfaces of the piezoelectric chip to ensure secure electrical connections throughout the testing procedure. The top of the platform supporting the piezoelectric chip is connected to an upper steel plate with dimensions of 12 cm × 12 cm × 1.0 cm via the spring baffle, which enables the upper plate to move freely within the frame composed of the four angle brackets under an applied load, while the spring serves as a vibration damper to ensure that the piezoelectric device responds only to the applied load, rather than secondary vibrations arising from that load. Therefore, the applied load is transmitted directly to the centerline of the piezoelectric device via the spring baffle. In addition, mass blocks of 800 g each can be added to the upper plate to facilitate the application of static loads to the centerline of the piezoelectric chip independently of the applied oscillatory load.

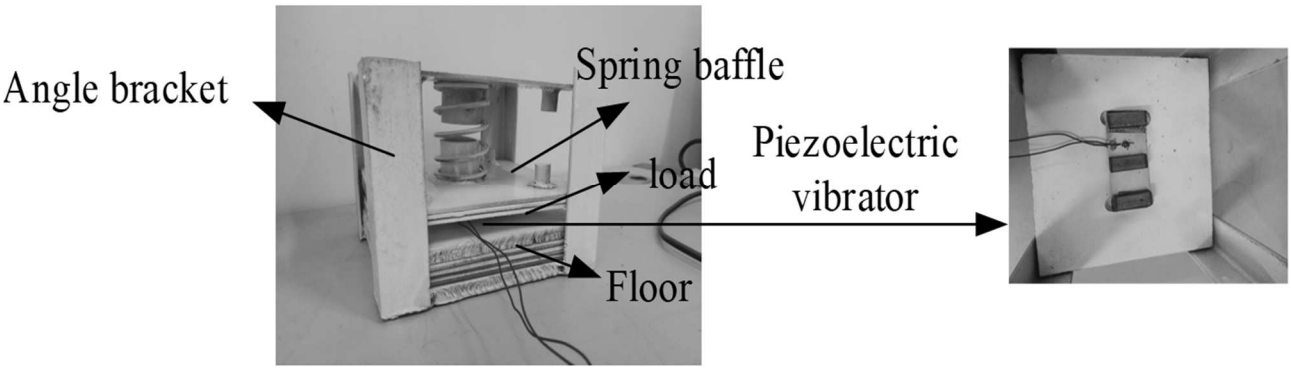

Fig. 3 *Variable excitation application device structure*

Tab. 1 *Performance parameters of piezoelectric device*

Substrate material	PZT material	Output voltage	Output current	Direct capacitance	Resonant impedance
Brass #CW67N	P81	0–48 VDC	0–12 mA	365–395 nF	<100 oHm

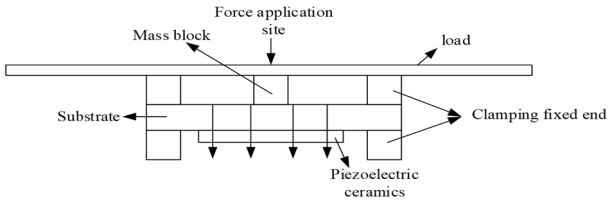

Fig. 4 *Structure of the piezoelectric power generation device and its installation in the excitation application device*

Fig. 5 *Details of piezoelectric device installation*

2.1.3 Piezoelectric power generation mechanism

According to the above discussion, the piezoelectric chip is fixed on both sides, and the boundary conditions are therefore mechanical clamping, while the device is operated under an electrical short circuit condition. Therefore, the stress T and the electric charge density displacement D arising from an applied strain S can be given as follows. Among them, S represents the deformation of piezoelectric ceramics under load force.

$$\begin{cases} T = c^E S - e^t E \\ D = eS + \varepsilon^S E \end{cases} \quad (1)$$

Where:

c^E…The short-circuit elastic stiffness constant,

e^T…The transpose of the piezoelectric stress constant matrix,

E…The electric field strength,

ε^s…The piezoelectric constant under the clamped condition.

The above constants generally reflect the ratio of mechanical energy to electrical energy, and the strength of the piezoelectric effect arising from the conversion of mechanical energy to electrical energy. The strength of this transformation is expressed by the electromechanical coupling coefficient. The strength of this transformation can also be expressed according to the mechanical loss, which is reflected by the mechanical quality factor Q_m defined as follows:

$$Q_m = 2\pi \frac{W_m}{\Delta W_m} \quad (2)$$

Where:

W_m…The mechanical energy per unit volume in each cycle of Piezoelectric device,

ΔW_m…The change in W_m over Piezoelectric device.

The mechanical energy consists of the kinetic energy E_k, gravitational potential energy P_g, and elastic potential energy P_e, which are respectively given as follows.

$$E_k = \frac{1}{2} m v^2 \quad (3)$$

$$P_g = mgh \quad (4)$$

$$P_e = \frac{1}{2} k v^2 \quad (5)$$

Where:

m…The mass,

v…The velocity,

g…The acceleration due to gravity,

h…The height of displacement,

k…Constant factor characteristic of the stiffness of the elastic body,

x…The displacement from equilibrium,

P_g…Gravitational potential energy,

P_e…The dynamic potential energy.

Applying the above analysis to the proposed experimental testing indicates that Q_m will vary according to the magnitude of a static applied load, and the frequency and amplitude of an oscillatory load. Therefore, the impacts of these factors on the maximum and minimum voltages of the piezoelectric chip output signal were considered in depth during the experimental testing process by applying oscillatory and static displacement components to the centerline of the piezoelectric chip of the form $x = h = A\sin(2\pi ft) + C_h$, where A is the amplitude of the oscillatory displacement, f is the frequency, t is time, and C_h is the static displacement component arising from the application of some arbitrary constant mass to the spring baffle. Accordingly, we note that $v = \mathrm{d}x/\mathrm{d}t = 2\pi fA\sin(2\pi ft)$. Therefore, the factors f and A affect E_k according to Equation (3), and an examination of Equations (4) and (5) indicate that the factors A and C_h affect P_g and P_e.

2.2 Static numerical analysis of the piezoelectric device

A three-dimensional (3D) model of the piezoelectric power generation device, including both the chip and substrate, and the mechanical mounting configuration shown in Fig. 6 was constructed using pro/Engineer computer aided design (CAD) software based on the dimensions of the actual physical device, and the resulting model was imported into the piezoelectricity module of the ANSYS software package, as shown in Fig. 7, and the performance characteristics of the piezoelectric device were simulated based on the PZT chip and substrate material characteristics listed in Table 2 under a pressure of 0.1 Pa with mechanical clamping boundary and electrical short circuit conditions at room temperature according to the methodology employed in previous studies [20-23].

Tab. 2 *Basic parameters of the piezoelectric chip and substrate materials used in the simulations*

Material	Young's modulus 10^{10} (N/m^2)	Density (kg/m^3)	Poisson ratio
Copper	11.2	8780	0.35
PZT	5.6	7500	0.36
Iron	12.0	7860	0.25

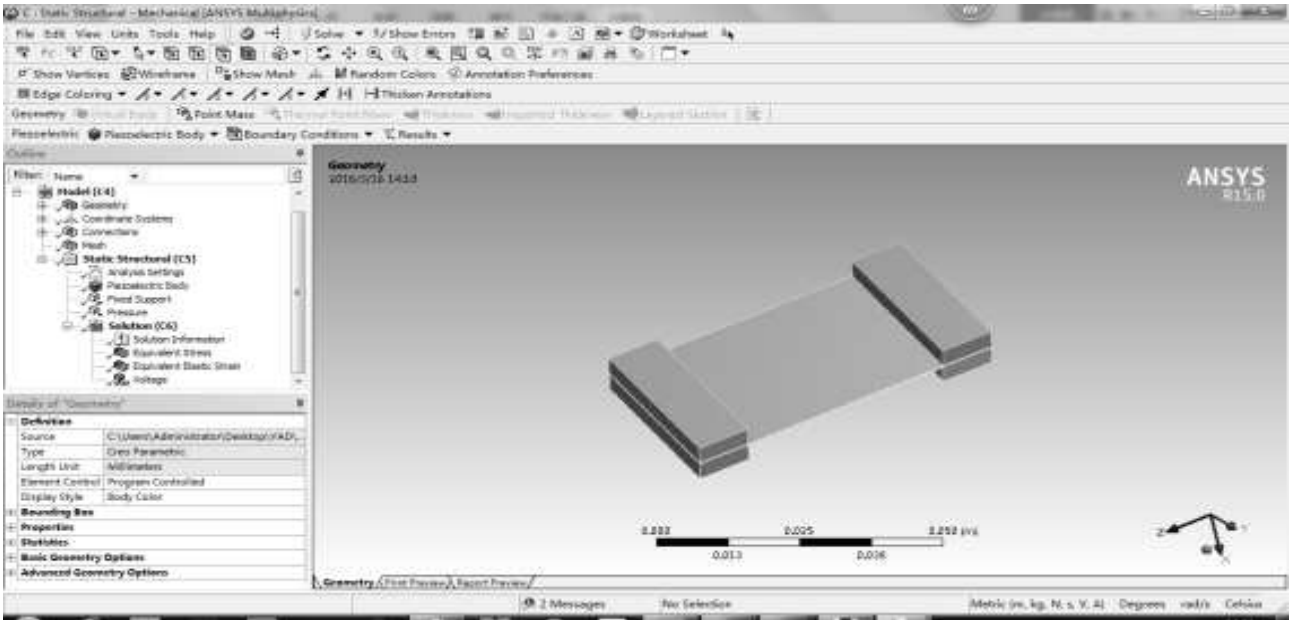

Fig. 6 *Geometric piezoelectric chip model and boundary conditions imported into ANSYS software*

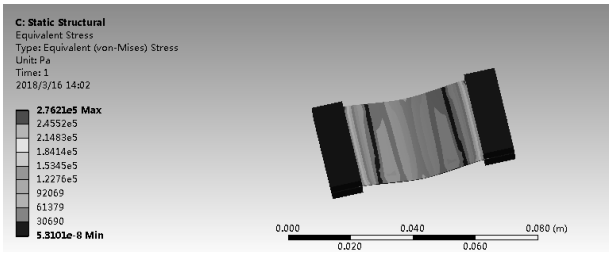

Fig. 7 *Equivalent stress distribution of the modeled piezoelectric device obtained under the standard applied load and boundary constraints*

The equivalent stress and equivalent elastic strain distributions obtained for the model under a standard static mechanical loading of Piezoelectric vibrator along the centerline of the chip are presented in Figs. 8 and 9, respectively. The figures indicate that the maximum stress and strain are generated at the fixed ends on both sides. Moving toward the center from the two sides, we note that the generated stress and strain initially decrease to minimum values at the quarter points, and then gradually increase toward the centerline of the device.

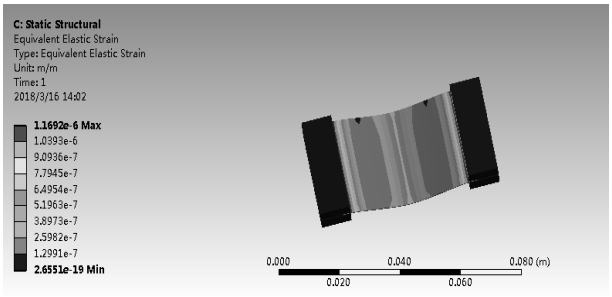

Fig. 8 *Equivalent elastic strain distribution of the modeled piezoelectric device obtained under the standard applied load and boundary constraints*

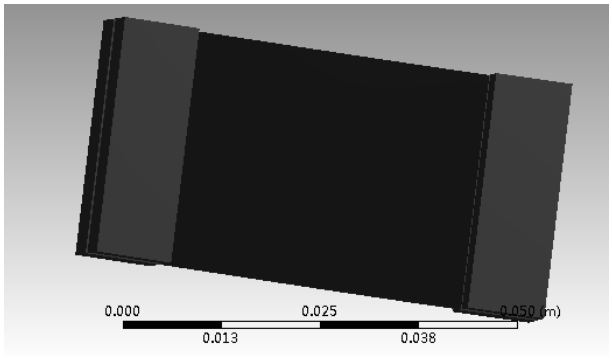

Fig. 9 *Voltage cloud image of the piezoelectric device obtained under an applied force of 0.1 N*

The fundamental properties of the P81 PZT material were input into the piezoelectricity module of the ANSYS software package according to the methodology employed in previous studies. These included the values of cE, e, E, and es. With the application of a force to the centerline of the piezoelectric device, the software provided voltage cloud images, like that obtained for an applied force of 0.1 N shown in Fig. 10, from which the maximum voltages could be determined.

The maximum voltages obtained for applied forces of 0.1, 0.2, 0.3, 0.4, 0.5, and 0.6 N were approximately 9.0 mV, 9.5 mV, 10.2 mV, 12.2 mV, 13.6 mV, and 15.3 mV, respectively. The overall trend is clearly illustrated in Fig. 9, which indicates that the maximum voltage obtained by the device increases more or less linearly with increasing applied force. Through the simulation of the piezoelectric device, it can be seen that the power output of the piezoelectric device changes with the change of the force, which provides a theoretical basis for this paper to put forward the influence of the

excitation on the power output of the piezoelectric device and paves the way for the later experiments.

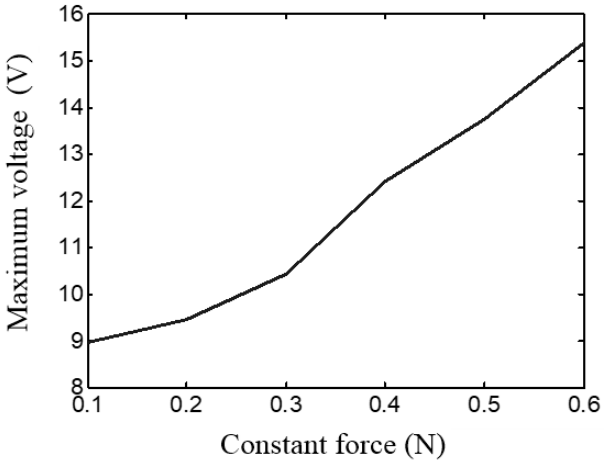

Fig. 10 *Maximum voltages of the piezoelectric device as a function of the applied static force to the centerline of the device*

3 Discussion of results

3.1 Experimental analysis of the piezoelectric device

The experimental vibration platform employed in the testing is shown in Fig. 11. The platform was mainly composed of an oscilloscope, computer, motor, transformer, governor, and the excitation application device. An eccentric shaft connected to the motor was placed at the central position at the top of the spring baffle to apply an oscillatory load with specified parameters to the centerline of the piezoelectric device. The signal response from the piezoelectric device was routed to the oscilloscope. However, the voltage signal transmitted from the piezoelectric device was heavily contaminated with noise. Therefore, the voltage signal was routed from the oscilloscope to the computer for noise suppression and analysis using MATLAB computer software according to the methodology employed in previous studies [24-30].

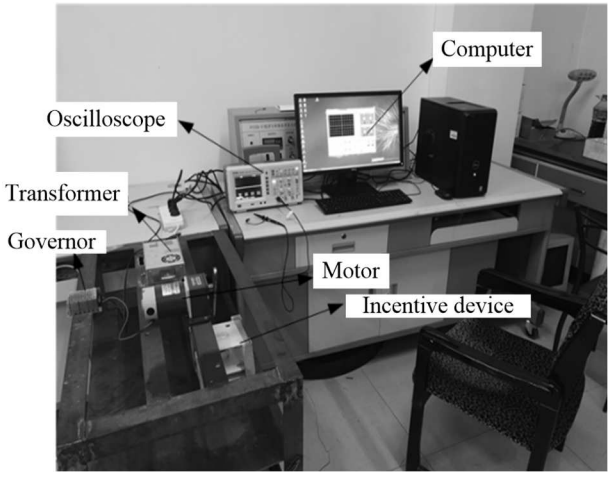

Fig. 11 *Experimental setup employed for device testing*

3.1.1 Results obtained under different mechanical excitation factors

The experimental conditions considered herein were an oscillatory load frequency of 1.0 Hz, 2.0 Hz, or 3.0 Hz, an oscillatory load amplitude of 1.0 mm, 2.0 mm, or 3.0 mm, and static loads of 1.6 N, 3.2 N, and 4.8 N arising from the application of a mass of 1600 g, 3200 g, or 6400 g to the spring baffle.

3.1.2 Impact of oscillatory load frequency

The impact of oscillatory load frequency on the periodicity, and the maximum and minimum voltages of the piezoelectric output signal were evaluated at 1.0 Hz, 2.0 Hz, and 3.0 Hz with an oscillatory load amplitude of 1.0 mm and static mass loading of 1600 g. The denoised waveforms obtained during the testing process for frequencies of 1.0 Hz, 2.0 Hz, and 3.0 Hz, and are more formally plotted as voltage versus time over a period of 2.4 s in Fig. 11(a), (b), and (c), respectively.

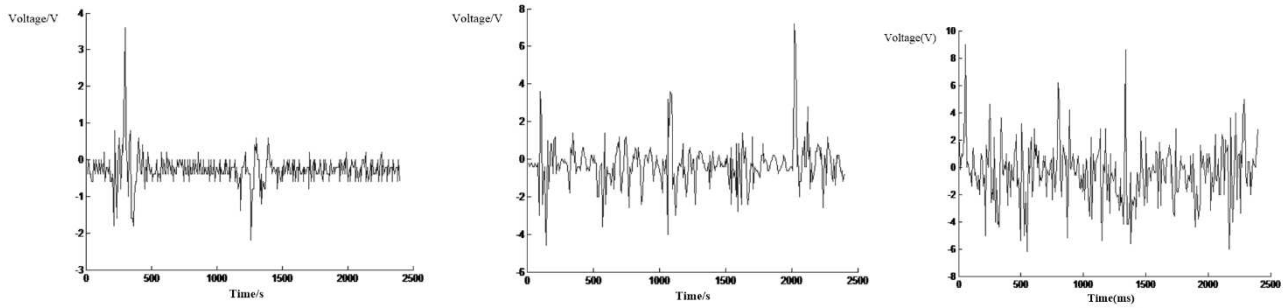

(a) *Frequency of 1.0 Hz* (b) *Frequency of 2.0 Hz* (c) *Frequency of 3.0 Hz*

Fig. 12 *Denoised voltage versus time waveforms obtained from the piezoelectric device under mechanical excitation with different frequencies (amplitude: 1 mm; static load: 1600 g)*

It can be seen from the results in Fig. 12(a) obtained at a frequency of 1.0 Hz that voltage waveforms are generated at intervals of about 1000 ms, where a maximum voltage of 2.2 V is generated at about 1400 ms and a minimum voltage of −4.4 V is generated at about 2100 ms, which represents a peak-to-peak maximum voltage value of 6.6 V. We further note from Fig. 12(b) obtained at a frequency of 2.0 Hz that voltage waveforms are generated at intervals of 500 ms, where a maximum voltage of 8.0 V is generated at

about 2100 ms and a minimum voltage of −4.5 V is generated at about 100 ms, which represents a peak-to-peak maximum voltage of 12.5 V. Finally, the results in Fig. 12(c) obtained at a frequency of 3.0 Hz indicate that voltage waveforms are generated at intervals of 250 ms, where a maximum voltage of 9.0 V is generated at about 1400 ms and a minimum voltage of −6.0 V is generated at about 600 ms, which represents a peak-to-peak maximum voltage of 15 V.

The maximum peak-to-peak voltages and waveform periodicities obtained from the above analyses are plotted in Fig. 13(a) and (b), respectively, as functions of the oscillatory load frequency. It can be seen from the results that the peak-to-peak voltage increases monotonically with increasing oscillatory load frequency, and the observed waveform periodicities agree perfectly with the frequencies of the applied oscillatory load.

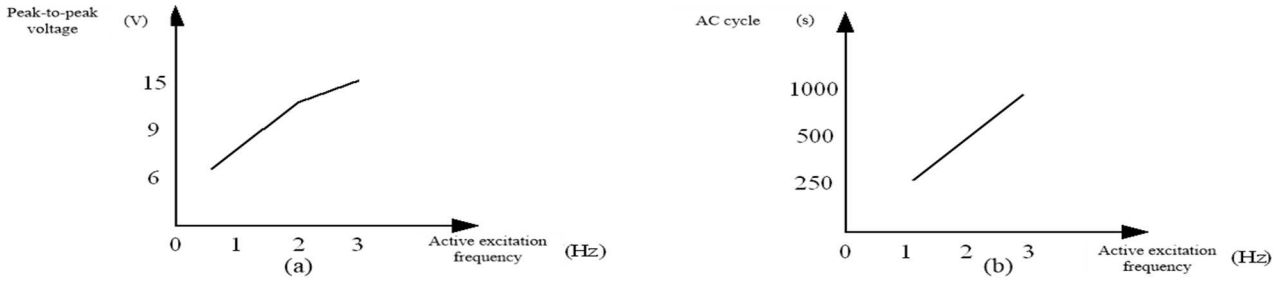

Fig. 13 *Maximum peak-to-peak voltages (a) and waveform periodicities (b) plotted with respect to the frequency of mechanical excitation*

3.1.3 Impact of oscillatory load amplitude

The impact of oscillatory load amplitude on the periodicity, and the maximum and minimum voltages of the piezoelectric output signal were evaluated at 1.0 mm, 2.0 mm, and 3.0 mm with an oscillatory load frequency of 1.0 Hz and static mass loading of 1600 g. The denoised waveforms obtained during the testing process for frequencies of 1.0 mm, 2.0 mm, and 3.0 mm are presented, respectively, and are more formally plotted as voltage versus time over a period of 2.4 s in Fig. 14(a), (b), and (c), respectively.

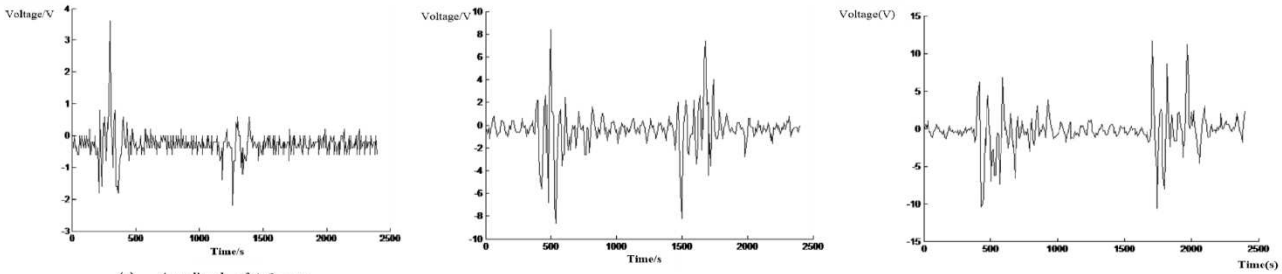

Fig. 14 *Denoised voltage versus time waveforms obtained from the piezoelectric device under mechanical excitation with different amplitudes (frequency: 1 Hz; static load: 1600 g)*

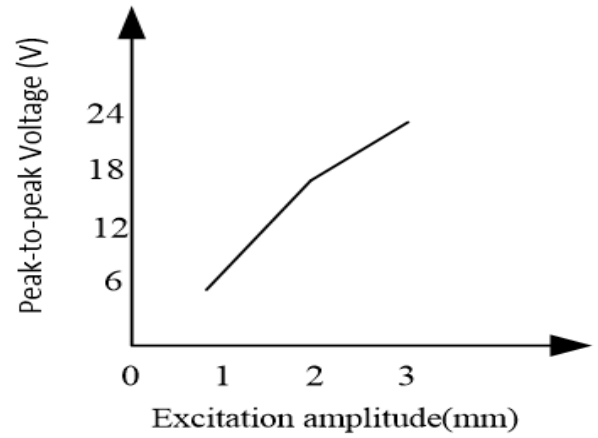

Fig. 15 *Maximum peak-to-peak voltages plotted with respect to the amplitude of mechanical excitation*

It can be seen from the results in Fig. 14(a), (b), and (c) that the amplitude of the oscillatory load has no effect on the periodicity of the captured waveforms, where waveforms are generated uniformly at intervals of about 1000 ms in accordance with the applied frequency of 1.0 Hz. We note from Fig. 13(a) obtained at an amplitude of 1.0 mm that a maximum voltage of 3.7 V is generated at about 300 ms and a minimum voltage of −2.2 V is generated at about 1300 ms, which represents a peak-to-peak maximum voltage value of 5.9 V. We further note from Fig. 14(b) obtained at an amplitude of 2.0 mm that a maximum voltage of 8.5 V is generated at about 500 ms and a minimum voltage of −8.5 V is generated at about 550 ms, which represents a peak-to-peak maximum voltage of 17 V. Finally, the results in Fig. 14(c) obtained

at an amplitude of 3.0 mm indicate that a maximum voltage of 12.5 V is generated at 1750 ms and a minimum voltage of −10 V is generated shortly after the maximum, which represents a peak-to-peak maximum voltage of 22.5 V.

The maximum peak-to-peak voltages obtained from the above analyses are plotted in Fig. 15 as a function of the oscillatory load amplitude. It can be seen from the results that the peak-to-peak voltage increases monotonically with increasing oscillatory load amplitude.

3.1.4 Impact of static loading magnitude

The impact of static loading magnitude on the maximum and minimum voltages of the piezoelectric output signal were evaluated at static mass loadings of 1600 g, 3200 g, and 6400 g with an oscillatory load frequency of 1.0 Hz and amplitude of 1.0 mm. The denoised waveforms obtained during the testing process for static mass loadings of 1600 g, 3200 g, and 6400 g are presented, respectively, and are more formally plotted as voltage versus time over a period of 2.4 s in Fig. 16(a), (b), and (c), respectively.

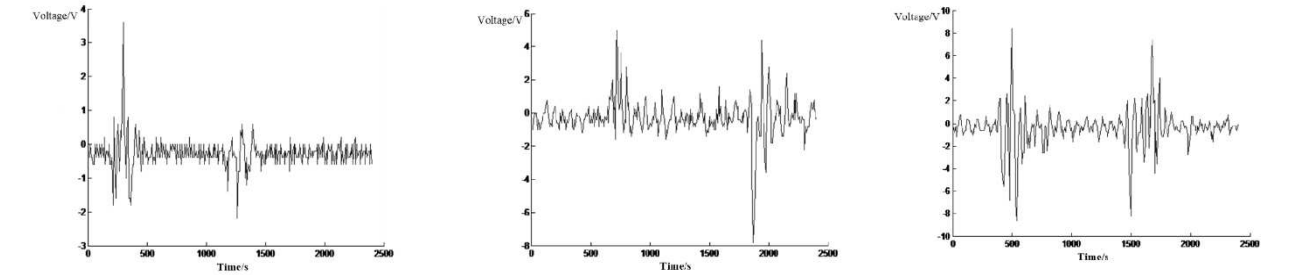

(a) *Image of voltage time function of 1600g mass with excitation load* *(b) Image of voltage time function of 3200g mass with excitation load* *(c)Image of voltage time function of 4800g mass with excitation load*

Fig. 16 *Voltage-time function image of different excitation loads*

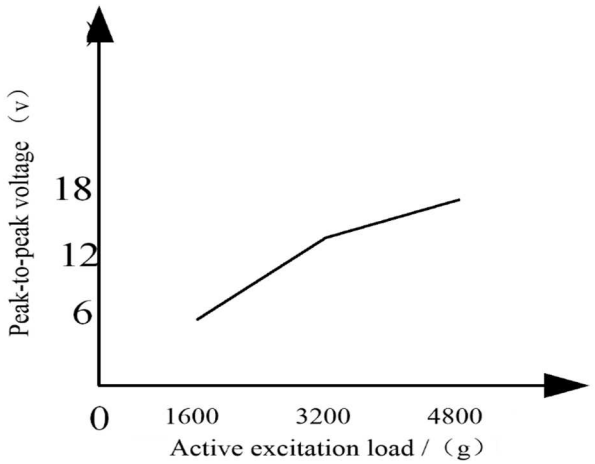

Fig. 17 *Maximum peak-to-peak voltages plotted with respect to the magnitude of static loading*

It can be seen from Fig. 16(a) obtained at a static load magnitude of 1600 g that a maximum voltage of 3.7 V is generated at about 300 ms and a minimum voltage of −2.2 V is generated at about 1300 ms, which represents a peak-to-peak maximum voltage value of 5.9 V. We further note from Fig. 16(b) obtained at a static load magnitude of 3200 g that a maximum voltage of 5.0 V is generated at about 700 ms and a minimum voltage of −9.0 V is generated at about 1800 ms, which represents a peak-to-peak maximum voltage of 13 V. Finally, the results in Fig. 16(c) obtained at a static load magnitude of 4800 g indicate that a maximum voltage of 8.3 V is generated at about 500 ms and a minimum voltage of −9.0 V is generated shortly after the maximum, which represents a peak-to-peak maximum voltage of 16.3 V.

The maximum peak-to-peak voltages obtained from the above analyses are plotted in Fig. 17 as a function of the magnitude of the static load. It can be seen from the results that the peak-to-peak voltage increases monotonically with increasing static loading.

The consistency of the obtained maximum peak-to-peak voltage values can be ascertained by comparing the values obtained independently under an oscillatory load with a frequency of 1.0 Hz and an amplitude of 1.0 mm in conjunction with a static mass loading of 1600 g, which yielded values of 6.6 V, 5.9 V, and 5.9 V in Subsections 3.2.1, 3.2.2, and 3.2.3, respectively. This yields an average value of 6.1 V with a standard deviation of just 0.3 V. Accordingly, we can conclude that the experimental results were consistent.

A comparison of Fig. 13(a), 15, and 17 demonstrates that increasing the oscillatory load frequency from 1.0 Hz to 3.0 Hz and increasing the static load magnitude from 1600 g to 4800 g had very similar impacts on the peak-to-peak voltage values obtained under those conditions, where the peak-to-peak voltages increased by about 150% in both cases. In contrast, the impact of an increasing oscillatory load amplitude from 1.0 mm to 3.0 mm on the obtained peak-to-peak voltages was quite profound, where the peak-to-peak voltages increased by nearly 270% over this range. These results may follow from our analysis in Subsection 1.3 of the factors affecting the components of mechanical energy of a piezoelectric device, where the frequency of the oscillatory displacement affects only the kinetic energy of the device, the static load affects

only the gravitational and elastic potential energies of the device, and the amplitude of the oscillatory displacement affects all three of these components. This is particularly the case for the kinetic energy and elastic potential energy of the device because these components involve the square of the velocity and displacement, respectively.

4 Conclusions

In this paper, a variable excitation piezoelectric power generation device is designed, which uses the mechanical energy generated by the vibration of the scraper conveyor to excite the piezoelectric energy capture device and convert it into electric energy to supply power for the sensor. Realized the continuous and stable self-power supply of the tension detection sensor of the scraper conveyor. Three different excitation modes are used to excite the piezoelectric vibrator, the influence of different excitation modes and degrees on the power generation characteristics of piezoelectric vibrators is analyzed. According to the influence of three different excitation modes on the generating voltage, it is concluded that the voltage generated by the generator is larger when the excitation frequency is 3r/s and the excitation amplitude is 3mm in this experiment. Therefore, in order to realize the power supply to the scraper chain tension sensor, the electric energy can be collected by increasing the external excitation frequency or selecting the part with higher external excitation frequency. In the future, more excitation methods such as space excitation can be studied to analyze the power generation characteristics of the piezoelectric vibrator, and more medium piezoelectric devices can be designed to improve the electromechanical conversion rate of the piezoelectric oscillator.

References

[1] TANG, H., (2014). Research on dynamic behavior of mining scraper conveyor ring chain drive system. *Guide To Getting Rich In Science And Technology,* Vol. 23, pp. 129-129.

[2] XU, G., YANG, W., (2009). Calculation and analysis of operating resistance of scraper conveyor. *Coal Mine Machinery*, Vol. 30, No. 01, pp. 3-5.

[3] MAO, J., SHI, J., ZHANG, D., WEI, X., (2008). Dynamic modeling and Simulation of heavy scraper conveyor. *Acta Coalae Sinica,* Vol. 33, No. 1, pp. 103-106.

[4] MAO, J., SHI, J., ZHANG, D., (2008). Simulation Research on automatic tension control system of scraper conveyor. *Journal Of System Simulation,* Vol. 20, No. 16, pp. 4474-4476.

[5] LI, W., MAO, J., LI, J., (2009). Research on the pretension regulating system of scraper conveyor. *Mining Machinery,* Vol. 7, pp. 11-14.

[6] LIU, K., XU, G., (2009). Design of chain tension measurement and control system for scraper conveyor. *Lifting And Transportation Machinery,* Vol. 08, pp. 53-55.

[7] LIU, P., YAN, F., (2008). Research on automatic monitoring system of scraper conveyor chain tension. *Coal Engineering,* Vol. 11, pp. 80-81.

[8] ZHANG, Q., WANG, H., MAO, J., ZHANG, D., YUAN, Z., (2015). Tension detection system of self powered scraper conveyor based on piezoelectric vibration energy capture. *Journal Of Sensing Technology,* Vol. 28, No. 09, 1335-1340.

[9] WILKIE, W.K., BRYANT, R.G., HIGH, J.W., FOX, R.L., HELLBAUM, R.F., JALINK JR, A., LITTLE, B.D., MIRICK, P.H., (2000). Low-cost piezocomposite actuator for structural control applications. *Smart Structures and Materials 2000: Industrial and Commercial Applications of Smart Structures Technologies. International Society for Optics and Photonics,* Vol. 3991, pp. 323-335.

[10] EGUSA, S., IWASAWA, N., (1993). Poling characteristics of PZT/epoxy piezoelectric paints. *Ferroelectrics,* Vol. 145, No. 1, 45-60.

[11] WIM, N., TAWEE, T., (2002). Properties of 0–3 Lead Zirconate Titanate–Polymer Composites Prepared in a Centrifuge. *Journal of the American Ceramic Society,* Vol. 85, No. 3, pp. 700-702.

[12] TANIMOTO T., (2007). A new vibration damping CFRP material with interlayers of dispersed piezoelectric ceramicparticles. *Composites Science and Technology,* Vol. 67, No. 2, pp. 213-221.

[13] CHO, J., ANDERSON, M., RICHARDS, R., BAHR, D., RICHARDS, C., (2005). Optimization of electromechanical coupling for a thin-film PZT membrane: I. Modeling. *Journal of Micromechanics and Microengineering*, Vol. 15, No. 10, pp.1797.

[14] BAKER, J., ROUNDY, S., WRIGHT, P., (2005). Alternative Geometries for Increasing Power Density in Vibration Energy Scavenging for Wireless Sensor Networks. *International Energy Conversion Engineering Conference*, pp.5617.

[15] JEON, Y.B., SOOD, R., JEONG, J.H., KIM, S.G., (2005). MEMS power generator with

transverse mode thin film PZT. *Sensors and Actuators A: Physical*, Vol. 122, No. 1, pp. 16-22.

[16] CHEN, K., ZHUO, J., LIU, W., HUANG, Y., HUA, C., ZHU, Q., YUAN, Y., (2024). Self-sensed, self-adapted and self-powered piezoelectric generator architecture by synchronous circuits of autonomous parameter tuning. *Energy Conversion and Management*, Vol. 300, p.117919.

[17] SATHASIVAM, K., GARIP, I., SHARIF, H., ABBAS, J.K., HUSSEIN, A.A., KHALEEL, S.K., RASOL, M.A., (2023). Developing a Piezoelectric Generator for Military Equipment–A Feasibility Study. *Electric Power Components and Systems*, Vol. 51, No. 17, 1859-1877.

[18] KIM, B.K., PARK, K.S., KEY, S.H., CHO, Y.S., (2023). Perovskite Relaxor-Dependent Contributions to Piezoelectric Power Generation of Multiple PZT Tape-Based Cantilever Structures at Nonresonant Frequency. *Advanced Energy Materials*, Vol. 13, No. 37, pp. 2301796.

[19] YU, X., SVIATOSLAW, K., NAN, W., (2023). Design and analysis of a 15 mode piezoelectric energy generator using friction-induced vibration. *Smart Materials and Structures,* Vol. 32, No. 3, p. 035040.

[20] IM, S., CHO, S.Y., CHO, J.H., HWANG, G.T., KINGON, A.I., BU, S.D., JO, W., KIM, S.H., JEONG, C.K., (2023). Study on relaxor polymer interface matrix for piezoelectric nanocomposite generators. *Applied Surface Science*, Vol. 613, p. 156031.

[21] WANG, J., TONG, Y., LI, C., ZHANG, Z., SHAO, J., (2022). A Novel Vibration Piezoelectric Generator Based on Flexible Piezoelectric Film Composed of PZT and PI Layer. *Polymers*, Vol. 14, No. 14, p. 2871.

[22] QIONGYAN, S., HUHAI, C., JIANG, L., (2021). The multi-harmonic excitation characteristic of airflow piezoelectric generator. *Journal of Vibroengineering,* Vol. 23, No. 5, pp. 1219-1229.

[23] KIM, S., HYEON, D.Y., HAM, S.S., YOUN, J., LEE, H.S., YI, S., KIM, K.T., PARK, K.I., (2021). Synergetic enhancement of the energy harvesting performance in flexible hybrid generator driven by human body using thermoelectric and piezoelectric combine effects. *Applied Surface Science*, Vol. 558, p. 149784.

[24] PENG, Y., XU, Z., WANG, M., LI, Z., PENG, J., LUO, J., XIE, S., PU, H., YANG, Z., (2021). Investigation of frequency-up conversion effect on the performance improvement of stack-based piezoelectric generators. *Renewable Energy*, Vol. 172, pp. 551-563.

[25] WEI, X., LIU, X., ZHENG, C., ZHAO, H., ZHONG, Y., AMARASINGHE, Y.W.R., WANG, P., (2021). A piezoelectric power generator based on axisymmetrically distributed PVDF array for two-dimension vibration energy harvesting and direction sensing. *Sustainable Energy Technologies and Assessments*, Vol. 44, p. 101001.

[26] WANG, Y., WU, S., WANG, Z., CHENG, T., BAO, G., (2021). Characteristics of Electric Energy Conversion in Pneumatic System Based on Piezoelectric Generator. *Journal of Energy Engineering*, Vol. 147, No. 2, p. 04021001.

[27] GĄBKA, J. (2023). Devising a Multi-camera Motion Capture and Processing System for Production Plant Monitoring and Operator's Training in Virtual Reality. *Manufacturing Technology*, 23, 399-417.

[28] SHI, Y., ZHU, Y., WANG, J. (2023). Surface Defect Detection Method for Welding Robot Workpiece Based on Machine Vision Technology. *Manufacturing Technology*, 23, 691-699.

[29] CZAN, A., CZANOVA, T., HOLUBJAK, J., NOVAK, M., CZANOVA, N., CZAN, A., KRISAK, D. (2024). Analysis of the Basic Characteristics of the Working Accuracy of the Atomic Diffusion Additive Manufacturing ADAM Process by Comparison with the Selective Laser Melting SLM Process. *Manufacturing Technology*, 24, 15-27.

[30] GEORGIA TECH RESEARCH CORPORATION. (2020). Patent Issued for Hybrid Generator Using Thermoelectric Generation and Piezoelectric Generation (USPTO 10,541,358). Electronics Newsweekly.